

# ACCURACY IMPROVEMENT OF ULTRASONIC INSPECTION FOR CIVIL STRUCTURES AND MATERIALS

Toshiyuki Oshima, Shuichi Mikami and Muhammad Saidur Rahman  
Department of Civil Engineering  
Kitami Institute of Technology  
165 Koen-cho, Kitami, Hokkaido, Japan

Motoharu Yasuda  
Tousetsu Doboku Consultants, Tokyo, Japan

Ronald. D. Kriz  
Virginia Polytechnic Institute and State University, Virginia

## INTRODUCTION

When we want to extend the life of an actual infrastructure and improve its serviceability adjusting the change of environmental situation, we need to evaluate its structural integrity quantitatively by using an appropriate inspection procedure on it. It is, therefore, important for a civil engineer to set up an effective inspection procedure to get the quantitative integrity evaluation of an infrastructure. The procedure of inspection for an infrastructure in Japan is divided into two types, that is, a periodical inspection and occasional (eventwise) inspection just after an earthquake. Inspector is chosen to have his experience career as a civil engineer more than 5 years and inspects infrastructures to classify the integrity level by five ranks on the each part of the structure by using the visual inspection according to the inspection manual tentatively provided by the Public Works Research Institute, Ministry of Construction. In the case if an inspector found any important damage or defect by the visual inspection, the precise inspection will be done by using a nondestructive testing to evaluate the size, shape and location of the damage or defect on the infrastructure. And if we could identify the damage or defect with an accurate information, we can evaluate its remaining life time by means of fracture mechanics and fatigue analysis and decide whether the damage or defect will propagate further or not. Thus we can, eventually, evaluate the structural integrity of the infrastructure by using the analysis of quantification theory [3] to classify the structures into four groups of integrity as A (Keep Watching), B (Need Small

Repair), C (Need Large Repair) and D (Need Replace or Reconstruction).

In this paper we discuss two subjects. One is on the 3D display of small defect in a fillet joint of welded steel structure and precise waveform analysis of the reflection wave of ultrasonic inspection. The another is on the analysis of material damping of concrete materials to improve the accuracy of internal information about the shape, type and length of cracks in the ultrasonic inspection of concrete.

### 3D DISPLAY OF SMALL DEFECT IN FILLET JOINT OF STEEL WELDING

#### Measurement System and Specimen

The measurement system employed in this paper is shown in Fig.1. The immersion type ultrasonic testing system is divided into two parts of subsystem and they are;

- 1) Image display system
- 2) Ultrasonic wave recorder system (Digital storage oscilloscope)
  - a) sampling speed up to 500 Mega samples per second
  - b) resolution of amplitude 10 bit
  - c) frequency range up to 300MHz

The sampling gate of the time axis is set corresponding to the thickness of specimen to receive first boundary echo from a defect and bottom echo. Ultrasonic wave recorder system can obtain the whole reflection waves that passed above mentioned time gate as 4096 data of digital values for every wave and display the spectrum of the detected waves by FFT.

In the steel plate specimen with 11.2mm thick fifteen artificial defects of different types are made by drilled holes as shown in Fig.2. Among them there are three types of diameter of drilled hole  $\phi$  as 4.0mm, 2.3mm, 1.6mm in fillet and butt joints.

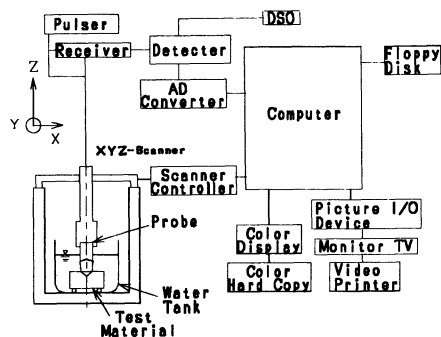


Fig.1. Measurement system.

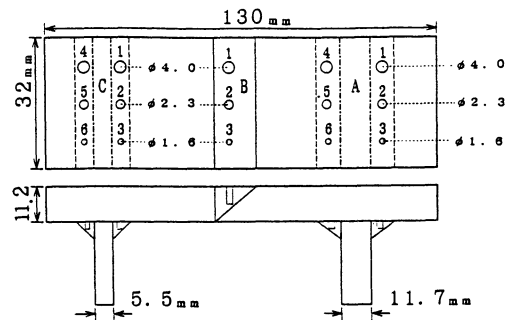
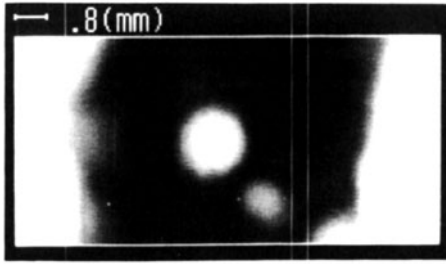
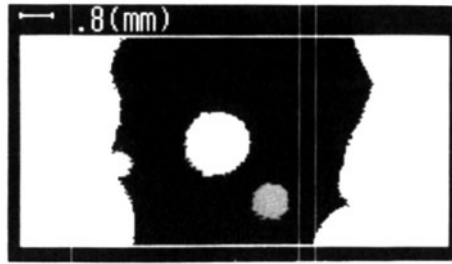


Fig.2. Specimens.



(a) Amplitude data



(b) Time of flight data

Fig.3.C-scan images.

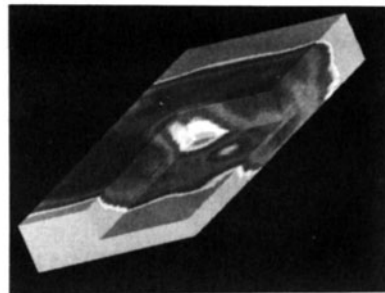
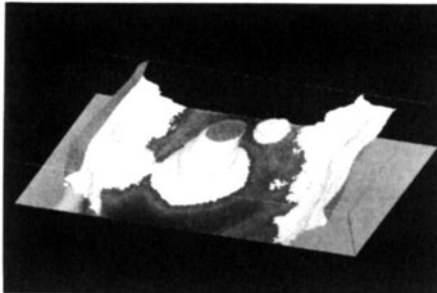


Fig.4. 3D image of defect A5.

### Detected Image of Defect Shape

By using an image display system we can obtain the maximum amplitude data which represent the distribution of maximum amplitude of echo reflected from the bottom surface of the welding or the boundary of a defect and the time of flight data which represent from where the incident wave returned back. And with these data we can get the C-scan images of maximum amplitude and time of flight with 256 grades of color display on 2D rectangular coordinate. One example of this C-scan image is shown in Fig.3. in the case of defect type A5 in Fig.2.

### 3D Display of Defect Shape

3D representation of maximum amplitude and time of flight data by using a computer graphics (CG) software on a workstation (WS) is shown here. The values of 256 color grades which correspond to the amplitude of echo and are on the 2D plane of scanning range, are taken in the vertical coordinate perpendicular to the above 2D plane. And the time of flight data are used like filtering of the boundary echo by which we can eliminate the scattering effect around a defect. By this filtering technique we can get

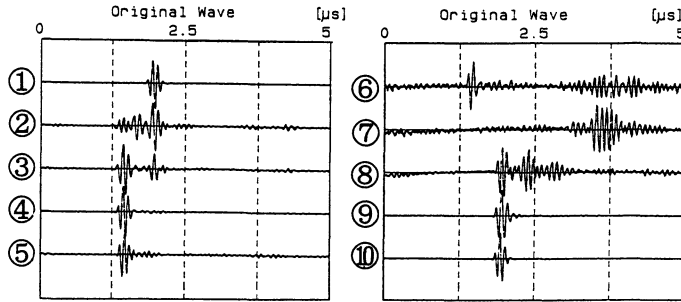


Fig.5. Measured waveforms of defect A1.

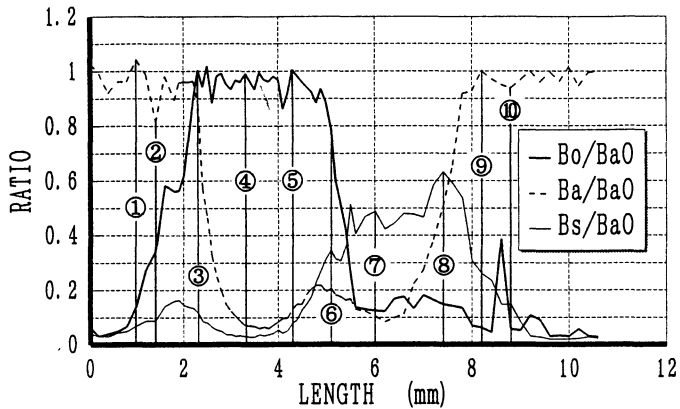


Fig.6. Results of (Bo/BaO) , (Ba/BaO) and (Bs/BaO) for defect A1.

the clearer 3D images of maximum amplitude data with clear boundary of small defect. In Fig.4 3D image of defect A5 (Fig.2) is shown. As shown in Fig.4 the defect A5 is embedded in a fillet joint and the diameter of the drilled hole is 2.3mm. By using AVS (Application Visualization System) of CG software we can rotate on the display to see the whole shape of defect in fillet joint. We call this type of display as "D-scope".

#### Precise Analysis of Boundary Echo By Waveform Analysis

It is, sometimes, difficult to get a good defect image because of wave scattering at the boundary of the defect. The scattering wave may be due to the variation of wave length and size and shape of defect. The focus of the 10MHz resonance frequency transducer adjusted on the center of the drilled hole then scans over the area of 10mm × 5mm at defect A1 (Fig.2). The reflection waves are obtained by line scanning with 100 μ m pitch along with the center line to across the defect A1. The original waves received are shown in Fig.5, where the transition of received waves from the bottom echo to the boundary echo is found. Waves ① and ⑨, ⑩ are reflected from the bottom surface outside of the welded area, waves ②, ⑥, ⑦, ⑧ reflected from the welded area and waves ③, ④, ⑤ reflected from the defect (drilled hole) area of the specimen. As the reflection wave has both the boundary echo and bottom echo, it is observed that when the transducer comes close to the defect tip the amplitude of boundary echo

becomes greater than bottom echo. Thus we can understand there is a boundary of the defect somewhere in the transition range.

The number shown in Fig.5 as ①, ② etc. indicates the location of transducer from where the reflection waves are taken and they also correspond to the location shown in Fig.6. Here we obtained maximum amplitude of boundary echo (Bo), bottom echo (Ba) and the normal maximum amplitude of bottom echo (BaO) is far from the defect boundary. We can observe from the ratio of Ba/BaO the undulations of the defect tips because they correspond to the distribution of the maximum amplitude of the boundary echo. The ratio of Bo/BaO is large around the defect tip where the ratio of Ba/BaO becomes small corresponding to the size of the real defect. We also observed that when the depth of defect is deep the Bo/BaO ratio becomes small at the boundary of the defect.

## MATERIAL DAMPING OF CONCRETE

By the recent demand for more reliable inspection and monitoring on concrete structures the Fiber-Optic Sensors for concrete is developed to embed longtime in the structures. [7,8] On the other hand impact-echo method is also well used to get internal information on concrete structures by analyzing precisely the received waves. [4,5,6] We need to get more accurate information on the size of crack, delamination of rebar, degradation of elastic property and strength and so on. And after any strong earthquake we have to estimate the size of damages and to design the appropriate repair on it. In NDC and NDE on concrete structures the pulse-echo method is well used and the received waves are precisely analyzed to identify the internal condition as an inverse problem. It is, in this case, important to know the effect of material damping characteristics of concrete on the ultrasonic wave propagation. So that the experimental results on the material damping of concrete are investigated in some cases of different volume fraction of each element of concrete.

### Measurement System and Specimen

The measurement system used in this experiment is shown in Fig.7. The peak frequency of transmitter (incident wave) is 50kHz and the surface wave and shear wave propagate along the specimen. The two types of receiving sensors are used and sensor V is longitudinal type and sensor H is shear type, respectively. The waves are received at two different location 1 and 2 as shown in Fig.7. The received waves are saved to wave memory with 25ns sampling pitch and 8kwords or 16kwords of 10bits depending upon the length of waves. The seven specimens of size  $30^{\text{mm}} \times 30^{\text{mm}} \times 400^{\text{mm}}$  are shown in Fig.8. Specimen PA is made with only cement paste. PB, PC, PD, and PE are made of gravel and cement paste. The average diameters of gravel are 10mm for PB and PC and 20mm for PD and PE, respectively, and the volume fractions of gravel are 10% for PB and PD and 30% for PC and PE, respectively. Specimens PF and PG are made of sand and cement paste and the volume fractions of sand are 30% and 50% for PF and PG, respectively. Water cement ratio is 50% in all cases.

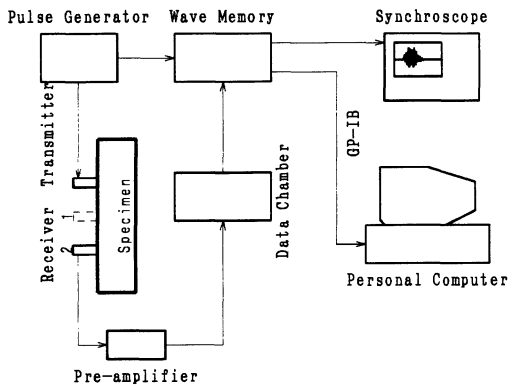


Fig.7 Measurement system.

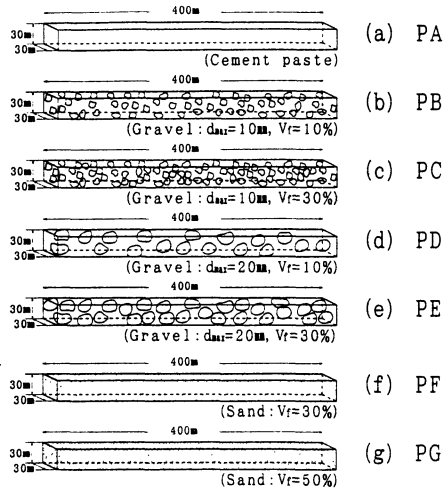


Fig.8. Specimens.

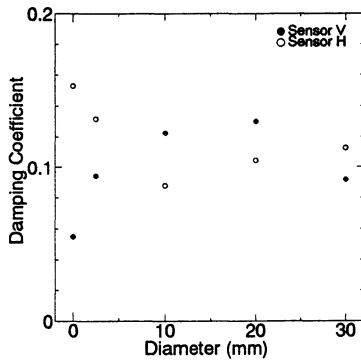


Fig.9 Effect of average gravel diameter on damping coefficient.

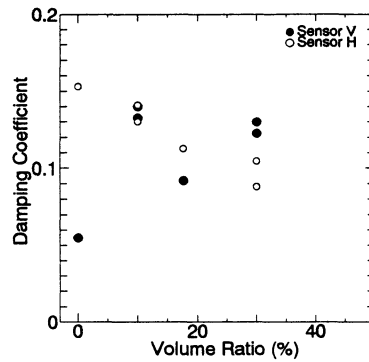


Fig.10. Effect of volume fraction of gravel in cement paste on damping coefficient.

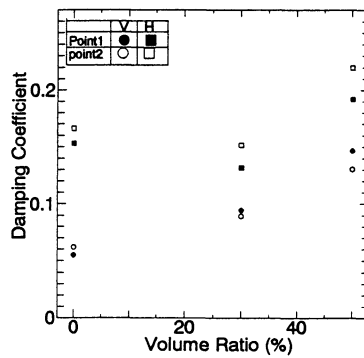


Fig.11. Effect of volume of sand on damping coefficient.

## Results

The effect of average gravel diameter damping on coefficient is shown in Fig.9 with two sensors V and H. In the case of sensor V which receives perpendicular displacement of wave to the surface of specimen, damping coefficient takes maximum value somewhere between 10mm and 20mm as diameter of gravel goes up. On the other hand in the case of sensor H which receives parallel displacement to the surface of specimen, damping coefficient takes minimum value as diameter is around 10mm. This data shown in Fig.9 is taken in the case of sensor location at 1 and the volume fraction of gravel as 30%.

The effect of volume fraction of gravel in cement paste on damping coefficient is shown in Fig.10. In the case of sensor V the damping coefficients increase as the volume ratios of gravel increase. And in the case of sensor H the damping coefficients decrease as the volume ratios increase and they intersect around at 20% of volume ratio.

The effect of volume fraction of sand on material damping is shown in Fig.11. The circular marks are obtained in the cases of sensor V and square marks are in the cases of sensor H at sensor location 1 and 2, respectively. In both cases the damping coefficients increase as the volume ratios of sand increase and in the cases of sensor H (shear type) the coefficients are larger than that of sensor H (longitudinal type).

## REMARKS

Summarizing the above results we have come to the concluding remarks as follows ;

To improve the accuracy of inspection on infrastructures two different results of experiment are shown. One result concerns 3D display of small defect in fillet joint of steel welding. By using AVS of computer graphics we can rotate the 3D display on the monitor of workstation to see the whole shape of defect. The combined system with ultrasonic testing and CG software gives us more useful information on a welding part of infrastructure.

And another result is about the material damping of concrete. The effect of average size and volume fraction of gravel and volume fraction of sand of cement paste on damping coefficient of concrete are analyzed in experimental research. The different characteristics of damping are obtained in the cases of longitudinal and shear type sensors with different wave modes.

## ACKNOWLEDGEMENTS

This study was supported in part by the Grant-in-Aid for Scientific Research from Japanese Ministry of Education, Science and Culture. The authors wish to thank Messrs Y.Ishikawa and T.Satoh, students of Kitami Institute of Technology, for their help in experimental study.

## REFERENCES

1. N.Sugawara, T.Oshima, S.Mikami, S.Sugiura : On the Accuracy Improvement in Ultrasonic Inspection by Using Computer Graphics and Waveform Analysis, Proc.of Japan Society of Civil Engineers, No.459/I-22,1993.
2. N.Sugawara, T.Oshima, S.Mikami, S.Sugiura : On the Accuracy Improvement of Small Defect for Ultrasonic Inspection by Using Scientific Visual Analysis, Review of Progress in Quantitative Nondestructive Evaluation, Vol.12, Ed. D.D. Thompson and D.E.Chimenti, 1993.
3. H.Mori, T.Oshima, S.Mikami, M.Honma,M.Funatsu : Effect of Individual Decision of Bridge Expert on Total Evaluation of Bridge Integrity, Journal of Constructional Steel, Vol.2, 1994.
4. N.J.Carino, M.Sansalone, N.H.Hsu : Flaw Detection in Concrete by Frequency Spectrum Analysis of Impact-Echo Waveforms, International Advances in Nondestructive Testing, Vol.12, 1986.
5. N.J.Carino, M.Sansalone : Flaw Detecting in Concrete using the Impact-Echo Method, NATO Advanced Research Workshop on Bridge Evaluation, Repair and Rehabilitation, 1990.
6. M.Sansalone, N.J.Carino : Detection Delaminations in Concrete Slabs with and without Overlays Using the Impact-Echo Method, ACI Materials Journal, Technical Paper, 1989.
7. A.Nanni, C.C.Yang, K.Pan, J.Wang, R.R.Michael, Jr. : Fiber-Optic Sensors for Concrete Strain/Stress Measurement, ACI Materials Journal, Technical Paper, 1991.
8. S.F.Masri, M.S.Agbabian, A.M.Abdel-Ghaffar, M.Higazy, R.O.Claus, M.J. de Vries : Experimental Study of Embedded Fiber-Optic Strain Gauges in Concrete Structures, ASCE, Vol.120, EM8, 1994.